

On the deep minimum state in the Seyfert galaxy MCG–6-30-15

Christopher S. Reynolds¹, Jörn Wilms^{2,3}, Mitchell C. Begelman^{4,5},
Rüdiger Staubert², and Eckhard Kendziorra²

¹*Dept. of Astronomy, University of Maryland, College Park, MD 20742, USA.*

²*Institut für Astronomie und Astrophysik, Abt. Astronomie, Universität Tübingen, Sand 1, 72076 Tübingen, Germany*

³*Dept. of Physics, University of Warwick, Coventry CV4 7AL*

⁴*JILA, Campus Box 440, University of Colorado, Boulder, CO 80309, USA.*

⁵*Department of Astrophysical and Planetary Sciences, University of Colorado, Boulder, CO 80309, USA.*

Submitted August 4th 2003

ABSTRACT

We present a detailed spectral analysis of the first observation of the Seyfert 1 galaxy MCG–6-30-15 by the European Photon Imaging Camera on board the *XMM-Newton* observatory, together with contemporaneous data from the Proportional Counter Array on the *Rossi X-ray Timing Explorer*. Confirming our previously published result, we find that the presence of extremely broadened reflection features from an ionized relativistic accretion disk is required even when one employs the latest X-ray reflection models and includes the effect of complex absorption. The extremely broadened reflection features are also present if the primary continuum is modeled with a thermal Comptonisation spectrum rather than a simple power-law continuum. With this fact established, we examine these data using a relativistic smearing function corresponding to a “generalized thin accretion disk” model. We find strong evidence for torquing of the central parts of the accretion disk (presumably through magnetic interactions with the plunging region of the disk and/or the rotating black hole itself). Indeed, within the context of these torqued disk models, this system appears to be in a torque-dominated (or “infinite-efficiency”) state at the time of this observation. In addition, we find marginal evidence that the X-ray emitting corona radiates a greater fraction of the total dissipated energy in the inner portions of the disk. We also perform a study of spectral variability within our observation. We find that the disk reflection features maintain roughly a constant equivalent width with respect to the observed continuum, as predicted by simple reflection models. Taken together with other studies of MCG–6-30-15 that find disk features to possess constant *intensity* at higher flux states, we suggest that the flux of disk features undergoes a saturation once the source emerges from a Deep Minimum state. We discuss the implications of these results for the physics of the Deep Minimum “state transitions”.

Key words: accretion disks – black hole physics – galaxies: individual (MCG–6-30-15) – galaxies: Seyferts

1 INTRODUCTION

Almost 40 years ago, it was suggested that the centres of galaxies host supermassive black holes and, further, that accretion onto those black holes powers active galactic nuclei (AGN; Salpeter 1964; Zeldovich 1964; Lynden-Bell 1969). Nowadays, the observational evidence in support of this picture is substantial. Proper motion studies of the stars in the centralmost regions of the Milky Way provide compelling evidence for the presence of a supermassive black hole with

a mass of about $3 \times 10^6 M_{\odot}$ (Eckart & Genzel 1997; Ghez et al. 1998, 2000, 2003; Eckart et al. 2002; Schödel et al. 2002). The kinematics of rotating central gas disks in several nearby low-luminosity AGN has also provided some of the most convincing evidence for supermassive black holes (for example, M87: Ford et al. 1994, Harms et al. 1994; NGC 4258: Miyoshi et al. 1995; Greenhill et al., 1995). Finally, spectroscopic studies of stellar kinematics reveal that almost all galaxies studied to date do indeed possess a central supermassive black hole. The very strong correlation between the

stellar velocity dispersion of a galaxy’s bulge and the mass of the black hole it hosts (Gebhardt et al. 2000; Ferrarese & Merritt 2000) argues for an intimate link between supermassive black hole and galaxy formation, a result of fundamental importance.

With the existence of supermassive black holes established, it is clearly of interest to study them in detail. While of crucial importance for establishing the presence of supermassive black holes, all of the kinematic studies mentioned above probe conditions and physics at large distances from the black hole, $r > 10^3 r_g$, where $r_g = GM/c^2$ and where M is the mass of the black hole. However, the energetically dominant region of an AGN accretion flow is very close to the central black hole, $r < 20 r_g$, where general relativistic effects become strong. This is the region we must consider if we are to truly understand these systems. Luckily, nature has provided us with an extremely useful probe of this region. X-ray irradiation of relatively cold material in the vicinity of the black hole can imprint characteristic features into the X-ray spectra of black hole systems, most notably the $K\alpha$ fluorescent line of iron. Detailed X-ray spectroscopy of these features can be used to study Doppler and gravitational redshifts, thereby providing key information on the location and kinematics of the cold material. This is a powerful tool that allows us to probe within a few gravitational radii, or less, of the event horizon. See Fabian et al. (2000) and Reynolds & Nowak (2003) for general reviews of relativistic iron line studies of accreting black holes.

The Seyfert 1 galaxy MCG–6-30-15 ($z = 0.008$) holds a special place in the history of relativistic iron line studies (e.g., see discussion in Reynolds & Nowak 2003). It was the first object for which observations by the *Advanced Satellite for Cosmology and Astrophysics (ASCA)* clearly revealed an iron emission line with a profile sculpted by strong relativistic effects (Tanaka et al. 1995; Fabian et al. 1995). Since then, studies of the iron line in this object have given us a window into some of the most exotic black hole physics observed to date. By identifying and then examining the so-called “Deep Minimum” state of this object, Iwasawa et al. (1996) used the iron line profile as measured by *ASCA* to demonstrate the need for iron fluorescence from within $r = 6 r_g$, the radius of marginal stability around a Schwarzschild black hole. This suggested that the central black hole was rapidly rotating (in order that the radius of marginal stability lie at $r_{ms} < 6 r_g$; Iwasawa et al. 1996, Dabrowski et al. 1997), although the possibility of fluorescence from within $r = r_{ms}$ prevented these arguments from being made rigorous (Reynolds & Begelman 1997).

More recently, *XMM-Newton* observations have provided strong support for the hypothesis of a rapidly rotating black hole. The first *XMM-Newton* observation of MCG–6-30-15 caught the object in a prolonged Deep Minimum state, allowing a high signal-to-noise spectrum to be obtained. The iron line was found to be extremely broadened and redshifted (Wilms et al. 2001; hereafter Paper I), in agreement with the previous results of Iwasawa et al. (1996). Using the scenario of Reynolds & Begelman (1997), even these new data could be (formally) described with emission around a non-rotating black hole. However, one would need essentially *all* of the emission to originate inside of $r = 3 r_g$, i.e. half of the radius of marginal stability. This is an unreasonable emission pattern in any current accretion model. Thus,

while uncertainties within the radius of marginal stability still hamper attempts to make these arguments absolutely rigorous, the data presented in Paper I make a compelling case that the supermassive black hole in MCG–6-30-15 is rapidly rotating.

The principal result of Paper I was the extreme central concentration of the iron line emission required to describe the observed breadth and redshift of the line profile. Even within the context of a rapidly-rotating Kerr black hole (with dimensionless spin parameter $a = 0.998$), a phenomenological model in which the line emissivity varied as a power-law in radius ($\epsilon \propto r^{-\beta}$) required an inner emitting radius of $r < 2.1 r_g$ and an emissivity index of $\beta = 4.7 \pm 0.3$. Assuming that the iron line emissivity tracks (even approximately) the underlying dissipation in the disk, this is in serious conflict with standard radiatively-efficient accretion disk models. In Paper I, we suggested that the central disk is being torqued by magnetic interaction with either the plunging region (Gammie 1999; Krolik 1999; Agol & Krolik 2000) or the rotating event horizon (Blandford & Znajek 1977; Li 2002). In both cases, the magnetic torque does work on the central accretion disk thereby producing a very centrally concentrated energy source.

In this paper, we further explore the *XMM-Newton*/EPIC data set first presented in Paper I. After describing our updated data reduction and calibration in Section 2, we present two distinct but related investigations. Firstly, in Section 3, we re-analyze the time-averaged X-ray reflection features investigated in Paper I. We show that the principal conclusions of Paper I, especially the need for a very high emissivity index, are robust to the application of a self-consistent ionized reflection model as well as the continuum curvature introduced by the inclusion of a physical thermal Comptonisation model or a complex absorber. By explicitly fitting the torqued disk model of Agol & Krolik (2000), we strengthen the hypothesis that this accretion disk is extracting the black hole’s spin energy. In Section 4, we proceed to examine variability of the iron line features. Our results for the Deep Minimum state are put into a wider context, and implications for models of this source are discussed, in Section 5.

Throughout this paper, we shall assume a Hubble constant of $71 \text{ km s}^{-1} \text{ Mpc}^{-1}$ (from the *Wilkinson Microwave Anisotropy Probe*; Spergel et al. 2003). The corresponding distance to MCG–6-30-15 is 32.9 Mpc ($z = 0.00779$; Reynolds et al. 1997), assuming negligible motion of this galaxy relative to the Hubble flow. All uncertainties are quoted at the 90% level for one significant parameter ($\Delta\chi^2 = 2.71$).

2 OBSERVATION AND DATA EXTRACTION

2.1 XMM-Newton Data Extraction

Our observation covered most of *XMM-Newton*’s orbit 108, on 2000 June 11/12, and was quasi-simultaneous with the *Rossi X-ray Timing Explorer* (RXTE). Here, we mainly report on data from the European Photon Imaging pn-camera onboard *XMM-Newton* (EPIC, Strüder et al., 2001, Turner et al., 2001), which was operated in its small window mode and the medium thick filter. The EPIC MOS-1 and MOS-2

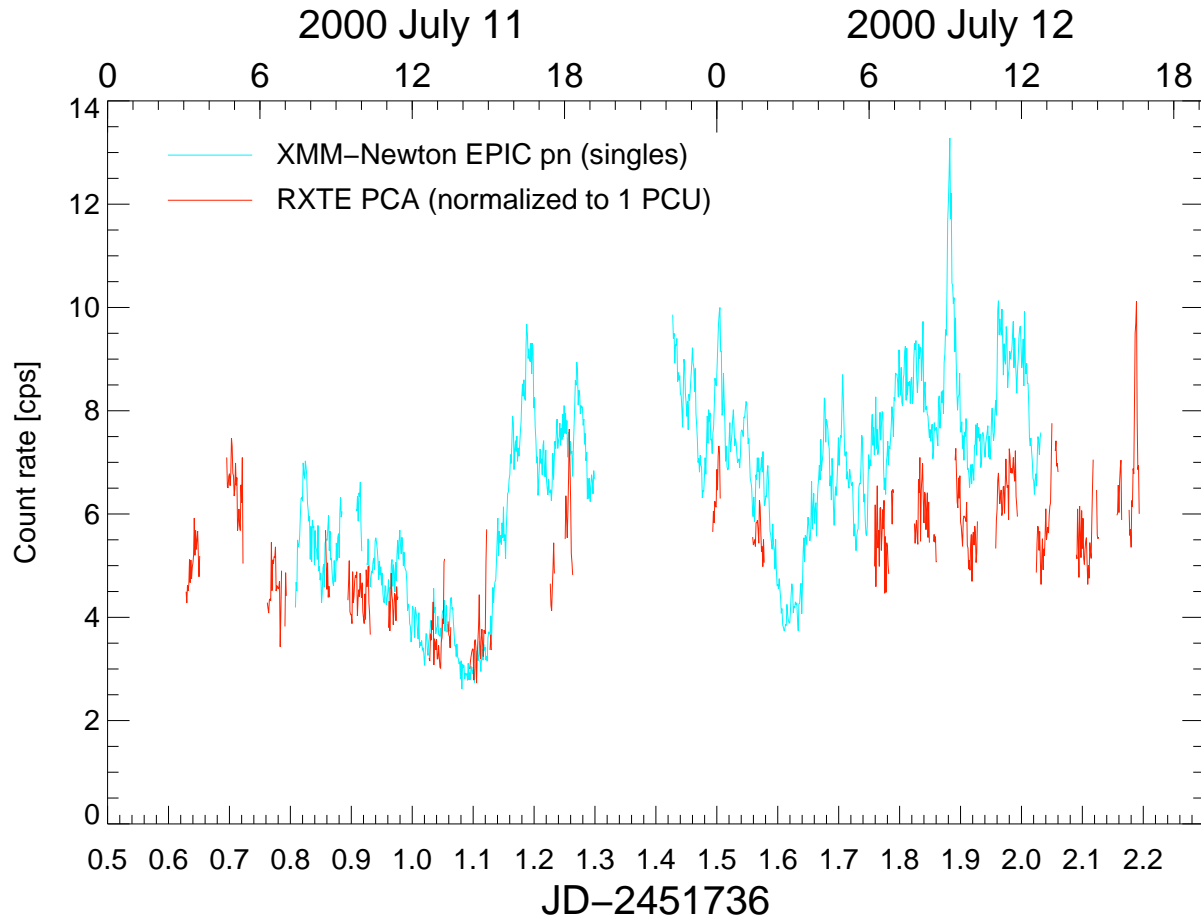


Figure 1. Lightcurves from the EPIC-pn (blue line) and RXTE-PCA (red line).

cameras were operated in the timing mode and the full-frame mode, respectively. Due to remaining calibration uncertainties of these cameras, we concentrate on the results from the EPIC-pn in this paper, and use the MOS-2 data only to check the instrument independency of our results. The data analysis was performed with version 5.3 of the *XMM-Newton* Science Analysis System (SAS) and with version 11.2.0 of XSPEC (Arnaud, 1996).

The source spectra and lightcurves were obtained from a circle with $40''$ radius centered on the source. We extracted spectra from single and double events separately, i.e., from events where all electrons produced by an X-ray photon are detected in a single EPIC-pn pixel or in two adjacent EPIC-pn pixels, respectively. As the energy-dependent distribution differs for single and for double events, modeling the data from both types of events separately allows us to check for the possible presence of pile-up in our data. Background data were extracted from a circle of the same area as the source data, but on a different position of the EPIC-pn to avoid the possible contamination of the background spectrum by out of time events, i.e., by photons registered during the read-out cycle of the EPIC pn. Since the background increases during the final part of the observation as *XMM-Newton* approaches the Earth’s radiation belts, the last 20 ksec of our observation are unusable. Furthermore, the telemetry gap due to the incomplete ground station coverage of *XMM-Newton*’s orbit during the early phase of the

mission is still present in our data (this situation has changed since then). The total EPIC-pn exposure time after the background screening is 112 ksec (with a “live-time” of 65 ksec).

The blue line in Figure 1 shows the 2–10 keV EPIC-pn lightcurve of MCG–6-30-15 for our observation. Since the source is strongly variable, in this paper we analyze data from both the overall observation, and from 10 ksec long data segments.

2.2 RXTE Data Extraction

As we mentioned above, observations with the Rossi X-Ray Timing Explorer (RXTE) were performed quasi-simultaneously with *XMM-Newton*. Starting before *XMM-Newton*, the RXTE observations cover most of the *XMM-Newton* observation, albeit with a much worse sampling due to the low Earth orbit of the satellite (Fig. 1, red line).

We extracted the RXTE data following standard procedures (employing LHEASOFT 5.2), using the newest instrument calibrations. To avoid times of high background count rates, only data taken more than 10 minutes after passages through the South Atlantic Anomaly were considered, with the additional constraint that the “electron ratio”, a measure for the particle background in the PCA, was less than 0.1. As MCG–6-30-15 is a rather faint source for the nonimaging instruments on RXTE, we concentrate on the data from RXTE’s low energy instrument, the proportional

counter array (PCA), only. Due to calibration uncertainties, only PCA data in the energy range from 3 keV to 15 keV were used.

3 THE TIME-AVERAGED “DEEP MINIMUM” SPECTRUM

In this section, we present a detailed re-analysis of the time-averaged EPIC-pn spectrum first presented in Paper I. The purpose of this re-analysis is two-fold. Firstly, we wish to test the robustness of the results from Paper I to the application of more realistic models. We will demonstrate that one still requires extreme broadening/redshifting of the X-ray reflection features, even when one uses self-consistent ionized reflection models (that include Compton broadening of the iron line), complex absorption, and a curved continuum derived from thermal Comptonisation. With that fact established, the second purpose of this section is to apply physically motivated relativistic smearing laws to these data, allowing us to test directly particular accretion disk models.

3.1 Modelling the 2–10 keV spectrum assuming an underlying power-law continuum

Initially, we consider only the 2–10 keV part of the spectrum and, furthermore, assume that the underlying continuum spectrum (i.e., prior to the effects of any reflection/reprocessing) is well described by a power-law. The restriction on the energy band is intended to avoid complexities associated with the well-known dusty warm absorber displayed by this object (Nandra & Pounds 1992; Reynolds 1997; Reynolds et al. 1997; George et al. 1998; Lee et al. 2001), as well as any oxygen and nitrogen recombination lines that may originate from the accretion disk (Branduardi-Raymont 2001; Sako et al. 2002). The power-law assumption is justified since, over this spectral range, almost all detailed models of thermal Comptonisation in AGN disk coronae predict a very good power-law form. The principal reason for this is that the 2–10 keV band is well above energies characterizing the seed photons (believed to be generically in the optical/UV/EUV band for AGN) but is well below the thermal cutoff of a typical disk corona (above ~ 100 keV). We shall relax both the energy restriction and power-law assumption later.

These spectral fits are reported in Table 1. All fits include absorption by the Galactic material along the line of sight to MCG–6-30-15 (with column density $N_{\text{H}} = 4.1 \times 10^{20} \text{ cm}^{-2}$; Elvis et al. 1989), modelled using the `tbabs` model of Wilms, Allen & McCray (2000). As shown in Paper I, a simple power-law is a poor fit, with residuals clearly indicating a rather narrow emission line at 6.4 keV in addition to a broad excess between 3–7 keV. The 6.4 keV feature is well fit by a narrow Gaussian, resulting in a formal measurement of $6.40_{-0.02}^{+0.01}$ keV for its energy. Thus, we can be secure in identifying this as the fluorescent $K\alpha$ emission line of iron which is in a rather low ionization state (less than Fe xvii).

As can be seen from Table 1, there are two rather different models that fit the EPIC-pn data equally well: the partial covering model and the relativistic ionized disk model.

This degeneracy can be broken by looking at the simultaneous higher energy data from the *RXTE*-PCA. To allow for any possible cross-calibration problems, we permit both the normalization and power-law index of the PCA spectral model to vary independently of the EPIC-pn spectral model. Indeed, we find that the PCA data require a photon index that is flatter by $\Delta\Gamma \sim 0.1$ than the EPIC-pn data, as is expected for the pre-LHEASOFT-5.3 PCA response matrix. Figure 2 shows the joint pn-PCA fit using each of these two spectral models. For completeness, these figures show the fit to the full 0.5–10 keV EPIC-pn band employing the “absorber+emitter” soft X-ray model discussed in the next section, although similar conclusions are reached by modelling just the 2–10 keV EPIC-pn spectrum in conjunction with the 3–15 keV PCA spectrum. It can clearly be seen that the partial covering model grossly fails to reproduce the spectrum of this source above 10 keV. To further examine this issue, we perform a joint pn-PCA fit of a combined spectral model that contains both relativistic disk features and partial covering. It is found that the column density of the partial absorber (assuming $f = 0.4$) has an upper limit of $N_{\text{H}} = 3 \times 10^{21} \text{ cm}^{-2}$ and is consistent with zero; we conclude that a partial absorber, if present at all, has a negligible effect on the part of the X-ray spectrum relevant to accretion disk studies.

Having shown that the partial covering model is not viable, we conclude that the spectral complexity in the 2–10 keV band of this source is primarily due to X-ray reflection from an ionized disk. The data require the disk component to be strongly broadened and redshifted. Our spectral model includes these effects by convolving the ionized reflection spectrum with the relativistic shifts expected from a thin accretion disk around a near-extremal Kerr black hole with dimensionless spin parameter $a = 0.998$ (Laor 1991). In addition to using updated calibrations, these fits extend the previous work reported in Paper I by employing the self-consistent models of X-ray reflection from ionized material by Ballantyne, Ross & Fabian (2001).

Confirming the principal result of Paper I, the degree of relativistic broadening required by these data pushes one to a high value of the emissivity index and a low value of the inner disk radius. If one fixes the inclination of the accretion disk at $i = 28^\circ$ (i.e., the value derived from ASCA data by Tanaka et al. 1995 and used in Paper I), the required emissivity index and inner radius are $\beta = 4.29_{-0.16}^{+0.15}$ and $r_{\text{in}} = 1.78_{-0.11}^{+0.14} r_{\text{g}}$, respectively. Allowing the inclination to be a free parameter, the best fitting values are even more extreme ($i = 56 \pm 4^\circ$, $\beta = 7.7 \pm 0.15$ and $r_{\text{in}} = 1.30_{-0.06}^{+0.21} r_{\text{g}}$).

3.2 Spectral fits to the 0.5–10 keV band

We proceed to discuss spectral fits to the full 0.5–10 keV band. This requires us to model the soft X-ray spectral features, a non-trivial task since the basic physics determining the soft X-ray spectrum (i.e., absorption vs. emission) is still the subject of much debate. However, since this work restricts itself to the medium resolution EPIC data, it is sufficient to model the soft X-ray complexity with phenomenological absorption/emission components (as opposed to constructing physical models of the absorber/emitter).

In this work, we employ two phenomenological models of the soft X-ray complexity. In the first model (which we

Model	Parameters	2–10 keV fitting	0.5–10 keV fitting (pure warm absorber)	0.5–10 keV fitting (absorber+emitter)
ABS(PO)	N_{H}	=4.1	$4.1^{+0.1}_{-0}$	$4.1^{+0.1}_{-0}$
	Γ	$1.795^{+0.015}_{-0.015}$	2.04 ± 0.01	1.82 ± 0.01
	χ^2/dof	2514/2109	5092/2905	3595/2902
ABS(PO+NFE)	N_{H}	=4.1	$4.1^{+0.1}_{-0}$	$4.1^{+0.1}_{-0}$
	Γ	$1.81^{+0.01}_{-0.02}$	2.05 ± 0.01	1.83 ± 0.01
	E_{narrow}	$6.40^{+0.01}_{-0.02}$	6.40 ± 0.01	6.39 ± 0.01
	$W_{\text{K}\alpha}$	65	96 ± 10	65 ± 15
	χ^2/dof	2401/2107	4870/2903	3474/2900
ABS*PCABS*(PO+NFE)	$N_{\text{H},1}$	=4.1	$4.1^{+0.01}_{-0}$	$4.4^{+1.3}_{-0.3}$
	$N_{\text{H},2}$	940^{+150}_{-160}	740^{+40}_{-30}	680 ± 50
	f	0.53 ± 0.03	$0.47^{+0.01}_{-0.02}$	0.41 ± 0.03
	Γ	$2.32^{+0.07}_{-0.06}$	2.26 ± 0.01	2.17 ± 0.04
	E_{narrow}	6.40 ± 0.01	6.40 ± 0.01	6.40 ± 0.01
	$W_{\text{K}\alpha}$	56 ± 10	60 ± 10	60 ± 12
	χ^2/dof	2063/2105	3077/2901	3041/2898
ABS(PO+NFE+cRECO)	N_{H}	=4.1	$4.1^{+0.1}_{-0}$	$4.1^{+0.1}_{-0}$
	Γ	$1.79^{+0.01}_{-0.02}$	2.17 ± 0.01	$1.88^{+0.01}_{-0.03}$
	E_{narrow}	$6.39^{+0.01}_{-0.01}$	$6.39^{+0.01}_{-0.03}$	$6.39^{+0.01}_{-0.03}$
	$W_{\text{K}\alpha}$	66^{+6}_{-12}	37 ± 9	56 ± 11
	\mathcal{R}	< 0.1	$5.9^{+0.5}_{-0.4}$	$0.89^{+0.21}_{-0.43}$
	χ^2/dof	2384/2106	3840/2902	3457/2898
	ABS(PO+NFE+KDISK[iREFL])	Γ	$1.76^{+0.04}_{-0.02}$	1.85 ± 0.01
E_{narrow}		6.40 ± 0.01	6.39 ± 0.01	6.39 ± 0.01
$W_{\text{K}\alpha}$		101 ± 25	96 ± 19	96 ± 18
$\log(\xi_{\text{broad}})$		$3.10^{+0.15}_{-0.20}$	$2.97^{+0.05}_{-0.03}$	$3.08^{+0.08}_{-0.09}$
r_{in}		$1.30^{+0.21}_{-0.06}$	$1.47^{+0.14}_{-0.08}$	$1.49^{+0.20}_{-0.10}$
β		7.70 ± 0.15	$5.7^{+1.3}_{-0.7}$	$5.5^{+1.2}_{-0.8}$
i		56 ± 4	44 ± 6	43^{+6}_{-10}
χ^2/dof		2060/2102	2983/2895	2976/2892

Table 1. First set of spectral fits to the time-averaged EPIC-pn data for the July 2000 observation of MCG–6-30-15. Spectral models are denoted as follows: ABS = neutral absorption with the Galactic column density of $N_{\text{H}} = 4.1 \times 10^{20} \text{ cm}^{-2}$; cRECO = cold reflection continuum (described by the PEXRAV model within the xspec fitting package; Magdziarz & Zdziarski 1995) with a relative reflection strength of \mathcal{R} ; iREFL = ionized reflection model (Ballantyne, Ross & Fabian 2001) with an ionization parameter ξ ; KDISK = relativistic smearing convolution model for a thin disk around a near-extremal Kerr black hole (spin parameter $a = 0.998$) viewed at an inclination of i with a surface emissivity varying as $\epsilon \propto r^{-\beta}$ between radii $r = r_{\text{in}}$ and $r = 400r_{\text{g}}$; NFE = narrow emission line of iron with rest-frame energy E_{narrow} and equivalent width $W_{\text{K}\alpha}$; PCABS = partial covering neutral absorber in which a column density N_{H} covers a fraction f of the X-ray source; PO = power-law continuum with photon index Γ

shall refer to as the “pure warm absorber”), we describe the soft X-ray structure as three simple absorption edges, with threshold energies and maximum optical depths that are left as free parameters in the spectral fits. Since these edges are not of physical interest in this work, we do not report their best fitting values in Tables 1–2. Typical threshold energies (and maximum optical depths) are $E \approx 0.73 \text{ keV}$ ($\tau \approx 0.70$), $E \approx 0.85 \text{ keV}$ ($\tau \approx 0.45$), and $E \approx 1.0 \text{ keV}$ ($\tau \approx 0.15$). These correspond closely with the expected absorption edges of O VII, O VIII, and Ne IX/Mg X. Blends of oxygen resonance absorption lines, as well as the L_3 -edge of neutral iron contained within dust grains embedded within the warm absorber, may also contribute to the first of these three edges.

The second soft X-ray model (the “absorber+emitter” model) consists of these three absorption edges plus relativistically-smearred soft X-ray emission lines of N VII and O VIII, with rest-frame energies of 0.50 keV and 0.65 keV,

respectively. These recombination lines are broadened according to the Kerr black hole accretion disk model of Laor (1991). Both the inclination and emissivity index describing the profiles of these soft X-ray recombination lines are allowed to vary as free parameters of the fit; in order to maintain generality, we do not fix them to be the inclination and emissivity index of the smearing function applied to the reflection features*. Although we do not report them, typical best-fitting equivalent widths for the N VII and O VIII lines are 0 eV (i.e., the line is not required) and 80 eV, respectively. Typical inclinations and emissivity indices characterizing the soft emission lines in our fits are $i = 38^\circ$ and

* Our goal here is to obtain an accurate but empirical *description* of the soft X-ray spectrum, not a physical model. We refrain from tying the parameters of the soft X-ray emission lines to the harder X-ray reflection features since, due to the superior photon statistics in the soft band, this would drive the entire spectral fit.

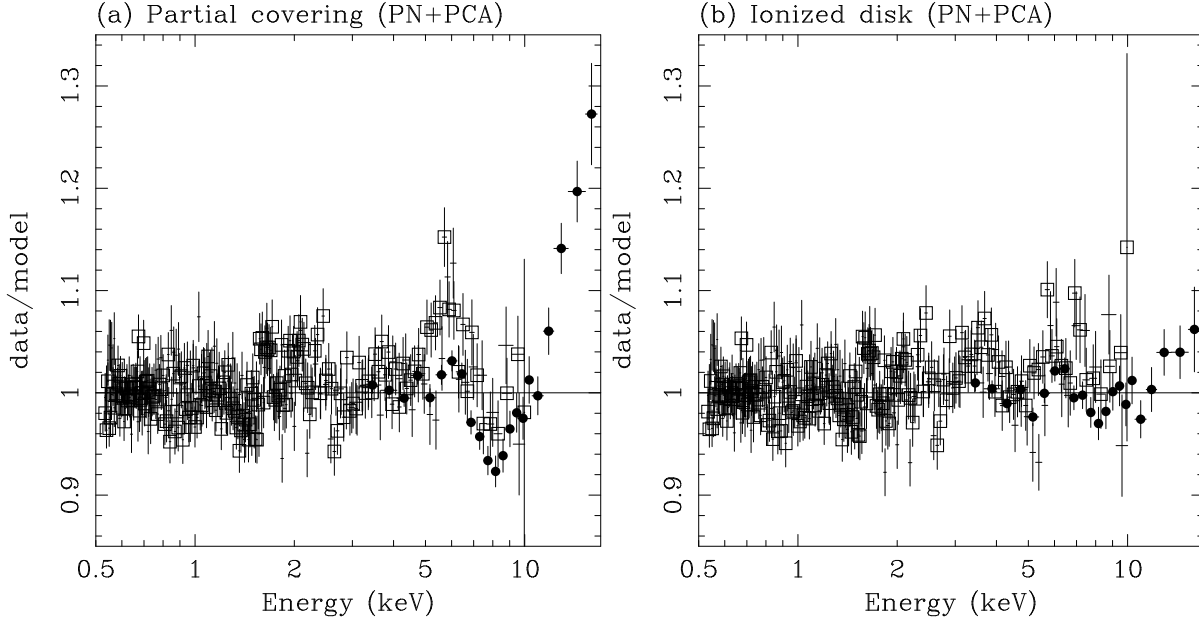


Figure 2. Fits of the joint EPIC-pn and RXTE-PCA data set with the partial-covering model (ABS*PCABS[PO+NFE]; panel a) and the relativistic ionized accretion disk model (ABS[PO+NFE+KDISK{iREFL}]); panel b). Although the partial covering model provides an adequate fit to the 0.5–10 keV EPIC-pn spectrum, it requires a rather steep underlying continuum (with photon index $\Gamma \sim 2.3$) which is in strong disagreement with the higher-energy spectral data from the PCA. On the other hand, the relativistic disk model adequately describes the joint pn-PCA spectrum from 0.5–17 keV. In both panels, the soft X-ray spectrum has been described using the “absorber+emitter” model from Section 3.2.

$\beta = 4.3$, respectively. We do not include any carbon recombination lines (which have also been discussed by Branduardi-Raymont et al. 2001, Sako et al. 2002 and Mason et al. 2003) since they all lie at energies below our low-energy cutoff.

From Table 1 it can be seen that the qualitative conclusions of the hard-band fits are robust to the inclusion of data down to 0.5 keV. Recalling that the partial-covering model fails when applied to the joint pn-PCA data, one can see that the only adequate fit is given by the relativistic ionized accretion disk model with a large emissivity index ($\beta \sim 5.5$) and a small inner radius ($r_{\text{in}} \sim 1.5r_g$). The principal difference between the 2–10 keV and 0.5–10 keV fits is the slightly lower inclination of the latter ($i = 44 \pm 6^\circ$ versus $i = 56 \pm 4^\circ$).

3.3 The effects of a curved continuum

In the above spectral fitting, we have assumed that the underlying X-ray continuum is strictly a power-law form. One might think that this would be a good assumption, since the observed band (0.5–10 keV) is much higher than the likely energy of the seed photons for the thermal Comptonisation (tens of eV) but much lower than the electron energy of a typical disk corona (100–200 keV). However, we must acknowledge the possibility that MCG–6-30-15 may be unusual in possessing a particularly cool corona. In this section, we assess the effect that the resulting continuum curvature would have on the inferred X-ray reflection as a function of radius in the disk.

For this study, we examine the 2–10 keV EPIC-pn data supplemented by the 3–15 keV RXTE-PCA data. Adding the 0.5–2 keV EPIC-pn data complicates the spectral fitting (since one must account for the soft X-ray absorption/emission) without improving the constraints. The ma-

ior limitation in the study of a curved continuum is the lack of readily available reflection models that can handle non-power law input spectra. We use the `compTT` model (Titarchuk 1994) in XSPEC to describe the continuum resulting from thermal Comptonisation. The seed photons are assumed to be characterized by a Wien spectrum with $kT = 50$ eV (typical of the optically-thick part of AGN disk). The temperature T and optical depth τ of the corona are left as free parameters. We then employ the `reflect` model (Magdziarz & Zdziarski 1995) in XSPEC to model the Compton reflection of this continuum spectrum from the disk surface. A narrow Gaussian emission line with a rest-frame energy in the range 6.40–6.97 keV is added to model the iron fluorescence line, and the whole spectrum is convolved with the `laor` (Laor 1991) kernel to describe the Doppler and gravitational redshift effects associated with the accretion disk.

This procedure constrains the temperature of the corona to be greater than $kT \sim 5.2$ keV; for coronal temperatures exceeding this, there is an almost perfect cancellation between spectral curvatures resulting from different coronal temperatures, reflection fractions and relativistic smearings. However, for all allowable coronal temperatures, a very steep emissivity index is required, $\beta > 3.9$. Freezing the emissivity index to be $\beta = 3$ resulted in a worsening of the goodness of fit parameter by $\Delta\chi^2 = 400$. Thus, our principal result is secure against the continuum curvature introduced by standard thermal Comptonisation models.

3.4 Physically motivated relativistic disk models

In the above discussion, we have examined these data with a variety of spectral models. We have found that the need for

Model	Parameters	2–10 keV fitting	0.5–10 keV fitting
ABS(PO+NFE+tTORQUED[iREFL])	Γ	$1.73^{+0.4}_{-0.3}$	$1.77^{+0.05}_{-0.04}$
	$\log(\xi_{\text{broad}})$	$3.21^{+0.14}_{-0.15}$	$3.19^{+0.21}_{-0.22}$
	r_{out}	$6.3^{+2.0}_{-1.4}$	$6.3^{+1.8}_{-2.0}$
	i	38 ± 4	38^{+4}_{-3}
	$\Delta\eta$	> 46	> 22
	χ^2/dof	2068/2103	2978/2891
ABS(PO+NFE+TORQUED[iREFL])	Γ	1.75 ± 0.2	$1.77^{+0.02}_{-0.07}$
	$\log(\xi_{\text{broad}})$	$3.19^{+0.25}_{-0.14}$	$3.21^{+0.11}_{-0.18}$
	i	< 27	< 27
	$\Delta\eta$	> 193	> 200
	χ^2/dof	2075/2104	2985/2892
ABS(PO+NFE+tPTDISK[iREFL])	Γ	$1.68^{+0.09}_{-0.02}$	$1.76^{+0.01}_{-0.05}$
	$\log(\xi_{\text{broad}})$	3.5 ± 0.1	$3.36^{+0.08}_{-0.15}$
	r_{out}	5.6 ± 0.9	$5.0^{+1.0}_{-0.7}$
	i	34^{+3}_{-4}	35^{+2}_{-4}
	χ^2/dof	2081/2104	2997/2892
ABS(PO+NFE+PTDISK[iREFL])	Γ	1.72 ± 0.02	$1.75^{+0.01}_{-0.02}$
	$\log(\xi_{\text{broad}})$	$3.72^{+0.05}_{-0.07}$	$3.55^{+0.07}_{-0.04}$
	i	< 8	< 6
	χ^2/dof	2169/2105	3166/2893

Table 2. Spectral fits to the MCG–6-30-15 EPIC-pn data with relativistic smearing functions corresponding to physical disk models, assuming an underlying power-law continuum. Abbreviations are: PTDISK = smearing model assuming an emissivity profile corresponding to a standard steady-state accretion disk (Novikov & Thorne 1974; Page & Thorne 1974) viewed at an inclination i ; tPTDISK = same as PTDISK except for the presence of an outer truncation radius at $r = r_{\text{out}}$, beyond which there is no X-ray emission or reprocessing; TORQUED = smearing model assuming an emissivity profile corresponding to a steady-state torqued accretion disk (Agol & Krolik 2000) viewed at inclination i with a torque-induced efficiency enhancement of $\Delta\eta$; tTORQUED = same as TORQUED except for the presence of an outer truncation radius at $r = r_{\text{out}}$, beyond which there is no X-ray emission or reprocessing. All other abbreviations are given in Table 1.

extreme relativistic effects is robust to different treatments of the soft X-ray complexity, complex absorption, and the use of a Comptonisation model instead of a simple power-law to describe the primary X-ray continuum.

Until now, we have employed a phenomenological model for the radial dependence of the disk emissivity, assuming that it can be described by a power-law form $\epsilon \propto r^{-\beta}$ truncated by inner and outer radii r_{in} and r_{out} . While this is an extremely useful parameterization, it does not correspond to any particular physical disk model. Given the quality of these data, we can go beyond these simple power-law emissivity profiles and attempt to constrain physical relativistic smearing models.

3.4.1 Theoretical framework

Firstly, we shall review some of the pertinent theory related to the geometrically-thin accretion disks of the type thought to be operating in Seyfert nuclei such as MCG–6-30-15. The standard thin disk model of black hole accretion was developed in a Newtonian setting by Shakura & Sunyaev (1973), and extended into a fully relativistic theory by Novikov & Thorne (1974) and Page & Thorne (1974; hereafter PT). In this model, the accretion disk is assumed to be geometrically-thin, radiatively-efficient, and in a steady-state. Furthermore, it is postulated that the disk experiences zero torque at the radius of marginal stability. With these assumptions, one can compute the dissipation rate, and hence

total radiative flux as a function of radius and black hole spin:

$$D_{\text{PT}}(r; a) = \frac{\dot{M}}{4\pi r} \mathcal{F}, \quad (1)$$

where we have defined the function \mathcal{F}

$$\begin{aligned} \mathcal{F} = & \frac{3}{2M} \frac{1}{x^2(x^3 - 3x + 2a)} \left[x - x_0 - \frac{3}{2}a \ln\left(\frac{x}{x_0}\right) \right. \\ & - \frac{3(x_1 - a)^2}{x_1(x_1 - x_2)(x_1 - x_3)} \ln\left(\frac{x - x_1}{x_0 - x_1}\right) \\ & - \frac{3(x_2 - a)^2}{x_2(x_2 - x_1)(x_2 - x_3)} \ln\left(\frac{x - x_2}{x_0 - x_2}\right) \\ & \left. - \frac{3(x_3 - a)^2}{x_3(x_3 - x_1)(x_3 - x_2)} \ln\left(\frac{x - x_3}{x_0 - x_3}\right) \right], \end{aligned} \quad (2)$$

with,

$$x = \sqrt{r/M} \quad (3)$$

$$x_0 = \sqrt{r_{\text{ms}}/M} \quad (4)$$

$$x_1 = 2 \cos\left(\frac{1}{3} \cos^{-1} a - \pi/3\right) \quad (5)$$

$$x_2 = 2 \cos\left(\frac{1}{3} \cos^{-1} a + \pi/3\right) \quad (6)$$

$$x_3 = -2 \cos\left(\frac{1}{3} \cos^{-1} a\right). \quad (7)$$

This dissipation profile is zero at $r = r_{\text{ms}}$ due to the zero-torque assumption, increases to a broad peak at $r \sim 1.5r_{\text{ms}}$,

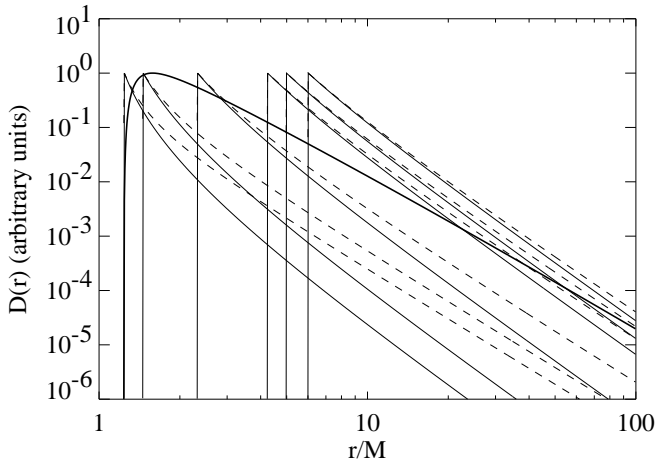


Figure 3. Model dissipation profiles for torqued time-independent accretion disks (using expressions from Agol & Krolik 2000). The thick line shows the dissipation profile for a standard non-torqued disk (i.e., one in which the ZTBC applies) around a near-extremal Kerr black hole with spin parameter $a = 0.998$. The thin solid lines show the torque-induced dissipation component D_{tor} for spin parameters of (from left to right) $a = 0.998, 0.99, 0.9, 0.5, 0.3$, and 0 . Note how the torque-induced dissipation profile becomes more centrally concentrated as the spin parameter is increased. The dashed lines show the torque-induced component of the emitted flux, including the effects of returning radiation. Figure from Reynolds & Nowak (2003).

and then declines as $\epsilon \propto r^{-3}$ at large radii (thick line in Fig. 3).

It has been realized in recent years that the assumption of zero-torque at the radius of marginal stability may be invalidated by magnetic connections between the Keplerian portion of the accretion disk and either the plunging region (i.e., the region $r < r_{\text{ms}}$) or the rotating event horizon itself (Krolik 1999; Gammie 1999; Li 2002, 2003). The formal generalization of the PT disk models including a (arbitrary) torque at $r = r_{\text{ms}}$ is given by Agol & Krolik (2000), who parameterized the extra torque via the corresponding enhancement in the radiative efficiency of the disk, $\Delta\eta$. The work done by the torque on the disk produces a new component to the disk dissipation that is very centrally concentrated,

$$D_{\text{tor}}(r; a) = \frac{3\dot{M}r_{\text{ms}}^{3/2}C_{\text{ms}}^{1/2}\Delta\eta}{8\pi r^{7/2}C(r)}, \quad (8)$$

where $C(r) = 1 - 3M/r + 2aM^{3/2}/r^{3/2}$ and $\Delta\eta$ is the additional disk efficiency induced by the torque (see Fig. 3). When this component is substantial, the overall dissipation profile is so concentrated that one can no longer ignore (even at a crude level) the effects of returning radiation (Cunningham 1975). In the limiting case of an infinite-efficiency disk (i.e., a disk that derives its whole luminosity from work done by the central torque) around a near-extremal Kerr black hole, as much as half of the radiation emitted from the disk can return to the disk via the action of strong light bending. Agol & Krolik (2000) showed that the effect of returning radiation is to produce an extra source of disk illumination described by the expression,

$$D_{\text{ret}}(r; a) \approx \frac{3M\dot{M}\Delta\eta R_{\infty}(a)}{8\pi r^3}, \quad (9)$$

where $R_{\infty}(a)$ is well described by the fitting formula given by Agol & Krolik (2000).

Thus, in this “generalized standard model” of thin-disk accretion onto black holes, the energy that is dissipated per unit proper time and per unit proper surface area is

$$D_{\text{tot}}(r; a) = D_{\text{PT}}(r; a) + D_{\text{tor}}(r; a). \quad (10)$$

Suppose that a fraction $f(r)$ of this energy is transported into a disk corona and hence radiated in the hard X-ray continuum (rather than as soft thermal emission from the optically-thick part of the accretion disk). If the corona is geometrically-thin then, with the exception of returning radiation, we need not consider light bending effects when deducing the X-ray flux that irradiates the optically-thick accretion disk (and hence gives rise to the observed reflection spectrum). Assuming that the corona is geometrically-thin and emits isotropically, the optically-thick disk will be irradiated by X-rays with an intensity,

$$I_{\text{X}}(r; a) = f(r) [D_{\text{PT}}(r; a) + D_{\text{tor}}(r; a)] + \bar{f}D_{\text{ret}}(r; a), \quad (11)$$

where \bar{f} is an appropriate averaging of $f(r)$ over the inner radii of the disk that contributes to the returning radiation. Given a functional form for $f(r)$, this irradiation profile can be used to construct the appropriately weighted relativistic smearing kernel that can then be convolved with the rest-frame reflection spectrum[†], thereby producing a full spectral model of smeared reflection from the disk.

3.4.2 Comparison of the generalized standard disk model with data

We now compare the EPIC pn data for MCG-6-30-15 with spectral models constructed from this generalized standard model of thin-disk accretion. However, we must first choose a functional form for $f(r)$, the fraction of the dissipated energy released in the irradiating X-ray continuum. Here, we choose the function form:

$$f(r) = \text{constant} \quad (r \leq r_{\text{out}}), \quad (12)$$

$$f(r) = 0 \quad (r > r_{\text{out}}), \quad (13)$$

$$(14)$$

where r_{out} can be considered as a “coronal truncation radius”. We also examine the situation in which $f(r)$ is a power-law in radius (see below).

Using this form for $f(r)$ in eqn. 11, we construct new relativistic smearing functions and hence a spectral model that can be compared with the data. This model (and indeed all models presented in the rest of this paper) assume a near-extremal Kerr black hole (with spin $a = 0.998$) and

[†] This procedure assumes that the rest-frame reflection spectrum (e.g., the ionization state of the surface layers) is constant across the whole disk. This is, of course, unlikely to be true in detail. However, the current data discussed in this paper are incapable of constraining models in which the underlying reflection spectrum changes as a function of radius.

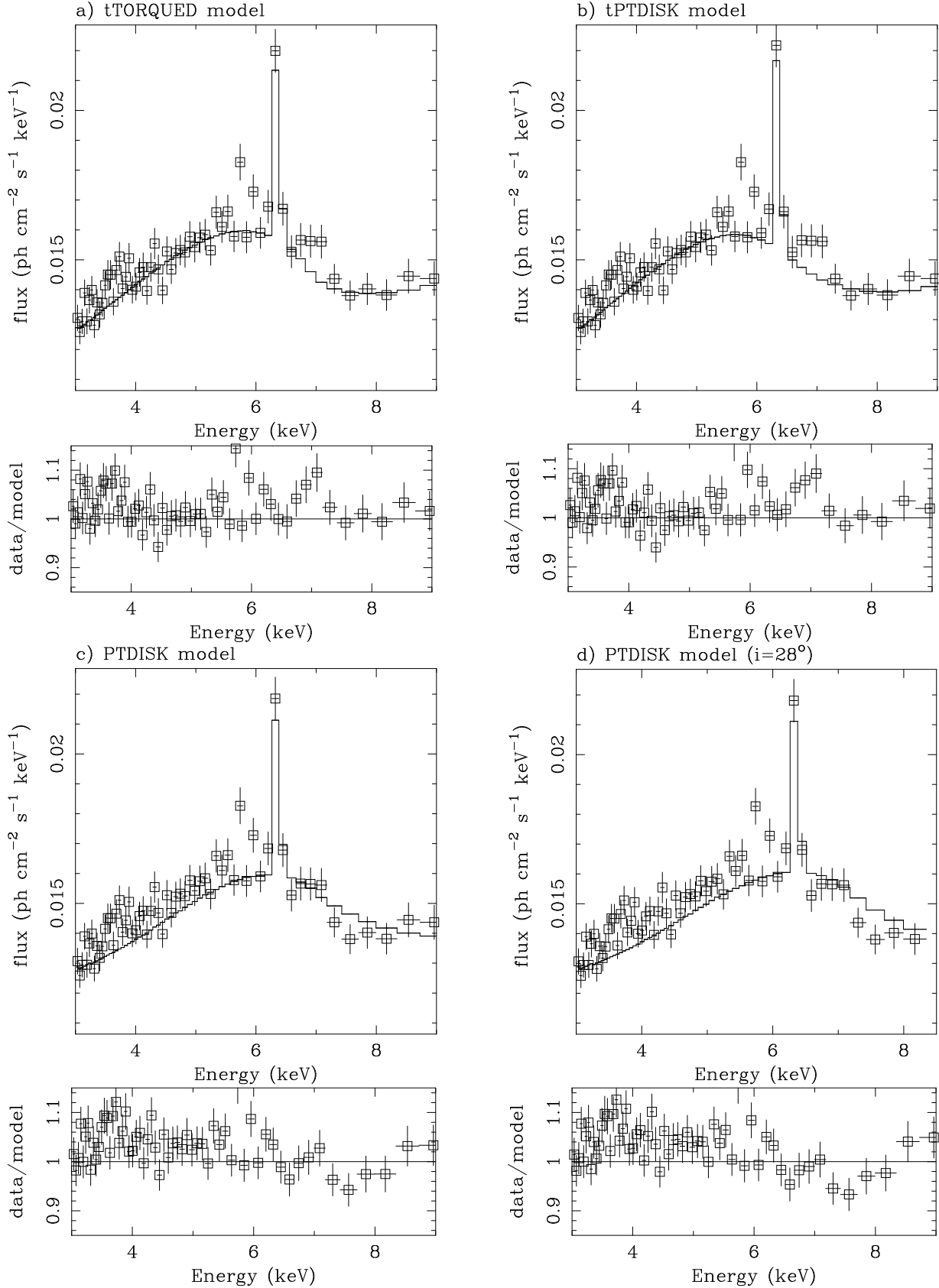


Figure 4. Fits of physical accretion disk models to the time average EPIC-pn spectrum of MCG-6-30-15. The fits displayed here were performed on the 2–10 keV data, although only the 3–9 keV range is shown for clarity. See Section 3.4 and Table 2 for details of these models and the fits.

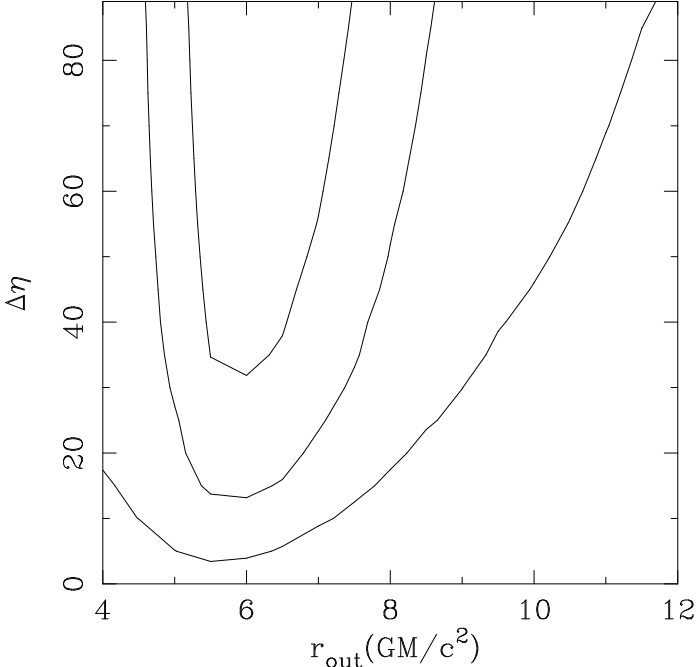


Figure 5. Confidence contours on the $(\Delta\eta, r_{\text{out}})$ -plane for the tTORQUED model applied to the time-averaged 2–10 keV EPIC-pn data. From top to bottom, contours are 68%, 90% and 95% for two interesting parameters. See Section 3.4 for details.

employ the Laor (1991) relativistic transfer function[‡]. We shall refer to the most general form of our model, where $\Delta\eta$ and r_{out} are free parameters, as tTORQUED (shorthand for truncated-TORQUED disk).

The results of fitting model tTORQUED to the EPIC pn data are reported in Fig. 4a, Fig. 5 and Table 2. Examination of the confidence contours in the $(r_{\text{out}}, \Delta\eta)$ -plane shows that, within the context of this model, the data require the disk to be both torqued (i.e., $\Delta\eta > 0$) and possess a finite coronal truncation radius at better than the 95% confidence level for two interesting parameters. In fact, the data require a very strongly torqued disk, with $\Delta\eta > 22$ (i.e., 2200%) at the 90% confidence level for one interesting parameter. In the language of Agol & Krolik (2000), the data argue for an “infinite-efficiency disk”, in which the dominant energy source is the black hole spin as opposed to gravitational potential energy of the accretion flow.

We explore the constraints imposed by these data further by restricting parameters of the tTORQUED model and examining the effect on the goodness-of-fit. Firstly, we consider the case in which the disk is subject to a torque at $r = r_{\text{ms}}$ but the corona is not truncated (i.e., $r_{\text{out}} \rightarrow \infty$; we refer to this as the TORQUED model). From Table 2, it can be seen that the goodness-of-fit parameter increases slightly ($\Delta\chi^2 = 7$ for one less degree of freedom in both the 2–10 keV and 0.5–10 keV fits). An application of the F-test suggests that this is a significantly worse description of these data at the 99.2% level. However, Protassov et al.

[‡] It would, of course, be desirable to construct models with arbitrary black hole spin. This, however, requires the calculation of an extensive set of new relativistic transfer functions, and is beyond the scope of this paper.

(2002) have pointed out that it is formally incorrect to use the F-test in this case; the TORQUED model lies on one boundary of the parameter space describing tTORQUED (the $1/r_{\text{out}} = 0$ boundary), and this fact can skew the probability distribution of the goodness of fit parameter. Due to this caveat, we consider that the evidence for coronal truncation is marginal.

Secondly, we assess the evidence for the presence of the inner torque at $r = r_{\text{ms}}$. If we impose the restriction that $\Delta\eta = 0$, we have an irradiation profile that follows a PT dissipation profile, albeit with an outer truncation radius. We refer to this model as tPTDISK. As reported in Table 2 (also see Fig. 4b), the goodness-of-fit parameter increases by $\Delta\chi^2 = 13$ upon the removal of this one degree of freedom from the models. The F-test implies that this is a significantly worse description of the data at the 99.97% level. Note that we do *not* impose the restriction that $\Delta\eta > 0$ in our tTORQUED fits and, hence, the restricted model tPTDISK does *not* lie on the boundary of the parameter space describing tTORQUED. Thus, the restriction on the application of the F-test raised by Protassov et al. (2002) does not apply here and we have no reason to distrust the F-test results. Hence, these data provide strong evidence for the presence of an inner disk torque.

We note that the best-fitting parameters of tPTDISK also might be inconsistent with the overall spectral energy distribution of MCG–6–30–15. The coronal truncation energy in these fits is constrained to be $r_{\text{out}} = 5.0^{+1.0}_{-0.7} r_g$, the same as the half-light radius of the accretion disk ($r_{1/2} \approx 5r_g$; Agol & Krolik 2000). Since 30–50% of the total radiative luminosity of this AGN is observed to emerge in the X-ray band (Reynolds et al. 1997), this result would imply an extremely high value of $f(r)$ (i.e., almost unity) in the inner disk.

We can also use this chain of reasoning to eliminate more extreme forms for the coronal dissipation fraction $f(r)$. In detail, we refit the tPTDISK model allowing $f(r)$ to have a power-law form, $f(r) \propto r^{-\lambda}$. The goodness of fit is close to that for the best-fit tTORQUED model. However, these fits require $\lambda > 2$ at the 90% confidence level. Noting the trivial fact that $f(r)$ cannot exceed unity, integration of the coronal dissipation across the disk implies that at most 3% of the dissipated energy can be released in the X-ray corona. Again, this violates the constraints on the total energetics of this source by a factor of 5, even once we include the fact that the instantaneous X-ray flux drops by a factor of 2 when the source enters the Deep Minimum state.

Finally, we examine the doubly restricted model PTDISK in which $\Delta\eta = 0$ and $r_{\text{out}} \rightarrow \infty$. From Table 2 it can be seen that this is a much worse fit to the data, with $\Delta\chi^2 = 101$ (upon the restriction of two model parameters) compared with the most general tTORQUED model. Indeed, it can be seen in Fig. 4c that the line profile visibly misses the data in the sense that it is insufficiently redshifted. Furthermore, the PTDISK model constrains the inclination to be less than 6° (8° if only the 2–10 keV data are considered). If we force the inclination to be 28° (the value deduced from the long ASCA observation of the “normal” state of this object by Tanaka et al. [1995]), the goodness of fit is *further* decreased by $\Delta\chi^2 = 38$ and $\Delta\chi^2 = 63$ for the 2–10 keV and 0.5–10 keV fits, respectively. In this case,

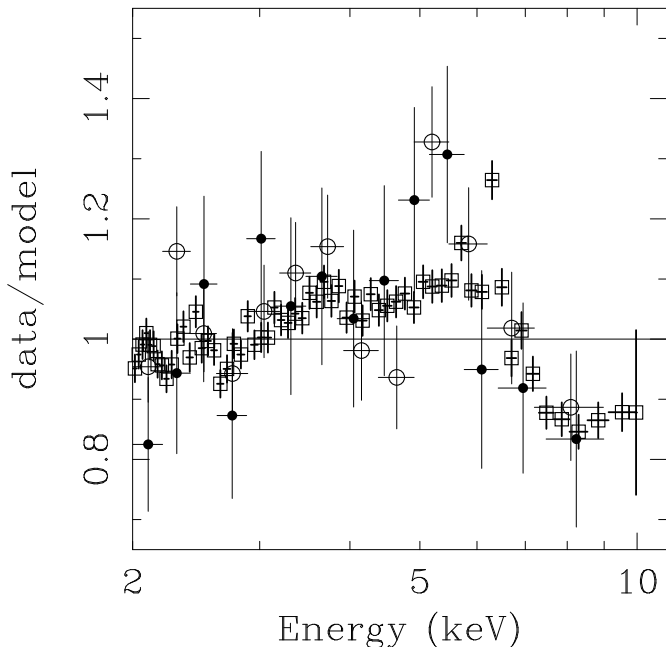


Figure 6. The filled and open circles show two representative difference spectra (for the 80–90 ksec and 100–110 ksec segments, respectively) ratioed against the best-fitting power-law model. The 10–20 keV segment has been used as our low-state spectrum when forming these difference spectra, although very similar results are obtained when we use the 20–30 keV data instead. Also shown is the time-average spectrum ratioed against the best-fitting power-law model (open squares). See Section 4 for a detailed discussion.

the systematic residuals in the fit are further exaggerated (Fig. 4d).

In summary, we construct relativistic smearing functions weighted by physically-motivated irradiation profiles whose parameters include the extra radiative efficiency $\Delta\eta$ due to the torque that is applied to the $r = r_{\text{ms}}$ (via MHD processes within the plunging region) and a coronal truncation radius r_{out} . We have found strong evidence that the disk is strongly torqued and, at this instant in time, may well be radiating primarily via the work done by this torque (a so-called infinite-efficiency disk). There is weaker evidence for a radial dependence of $f(r)$ which we model as a truncation of the corona at $r_{\text{out}} \approx 6GM/c^2$.

4 SPECTRAL VARIABILITY

With data of this quality, it is obviously interesting to search for spectral variability on the shortest timescales possible. Experimentation shows that an adequate spectrum requires an exposure of 10 ksec of data. In this section, we analyze spectral variability across eleven uniformly spaced 10 ksec segments of our observation. The median “live=time” for each of these segments is about 7 ksec.

Of particular interest, of course, is any variability of the iron line profile. We begin our investigation of iron line variability by examining “difference spectra”, following the work of Fabian et al. (2002) and Fabian & Vaughan (2003). In detail, we isolate and examine the variable part of the X-ray spectrum by subtracting the lowest flux spectrum from the other spectra. Since we are primarily interested in iron line

variability, we restrict our attention to the 2–10 keV region of the EPIC-pn spectrum. Figure 6 shows two representative difference spectra (for the 80–90 ksec and 100–110 ksec segments), using the 10–20 ksec segment of data as our representative lowest-state spectrum; the broad spectral feature that we interpret as reflection from a relativistic disk can be seen in both of these difference spectra. In fact, 8 of the 10 difference spectra show evidence for the very broad disk feature, with the remaining two spectra being too noisy to draw any conclusions. Furthermore, the narrow iron line does not appear in the difference spectra. In other words, the narrow iron line has a constant absolute flux, as expected if it originates from distant material.

Although they are rather noisy, the difference spectra suggest that (apart from the narrow iron line) the 2–10 keV EPIC-pn spectrum maintains the same overall shape during large changes in source flux once small variations in the underlying power-law index have been taken into account. In other words, the difference spectra imply that the broadened reflection features maintain a constant equivalent width relative to the underlying continuum, as opposed to a constant absolute intensity.

To investigate this further, we fit each spectrum with a power-law modified by Galactic absorption plus a simple broad iron line described by the `laor` model in XSPEC. These fits are much simpler than those discussed in Section 3 since we do not include the reflected X-ray continuum. We fix all parameters of the `laor` component apart from its intensity at the values derived by fitting this model to the time-averaged spectrum; $r_{\text{in}} = 1.24r_g$, $r_{\text{out}} = 400r_g$, $\beta = 6.4$, $i = 48^\circ$. Of course, the spectral feature of interest is a combination of both a broad iron line and the rather complex ionized reflection continuum — however, the simple broad line model allows us to measure a robust intensity for this feature as a whole. As shown in Fig. 7, there is indeed a correlation between the 2–10 keV continuum flux and the intensity of the broad disk feature such as to keep an approximately constant equivalent width.

Both the difference spectra and the direct spectral fitting shows that the equivalent width, not the absolute intensity, of the broad disk feature remains approximately constant throughout this observation. This is the behaviour expected within the disk reflection paradigm, but is at odds with the findings of previous investigations. We discuss this discrepancy and its possible resolution in Section 5.

It is also interesting to search for stochastic changes in the iron line profiles that are uncorrelated with the overall source flux. In Fig. 8 we show both the instantaneous 2–10 keV spectrum and the time-averaged 2–10 keV spectrum, ratioed against a simple power-law modified by Galactic absorption. While there are hints of numerous features popping in and out of the line profile (especially at ~ 4 keV), they are not statistically significant at the 90 per cent level and hence will not be discussed further. In fact, we find no gross changes in the velocity profile of the X-ray reflection features.

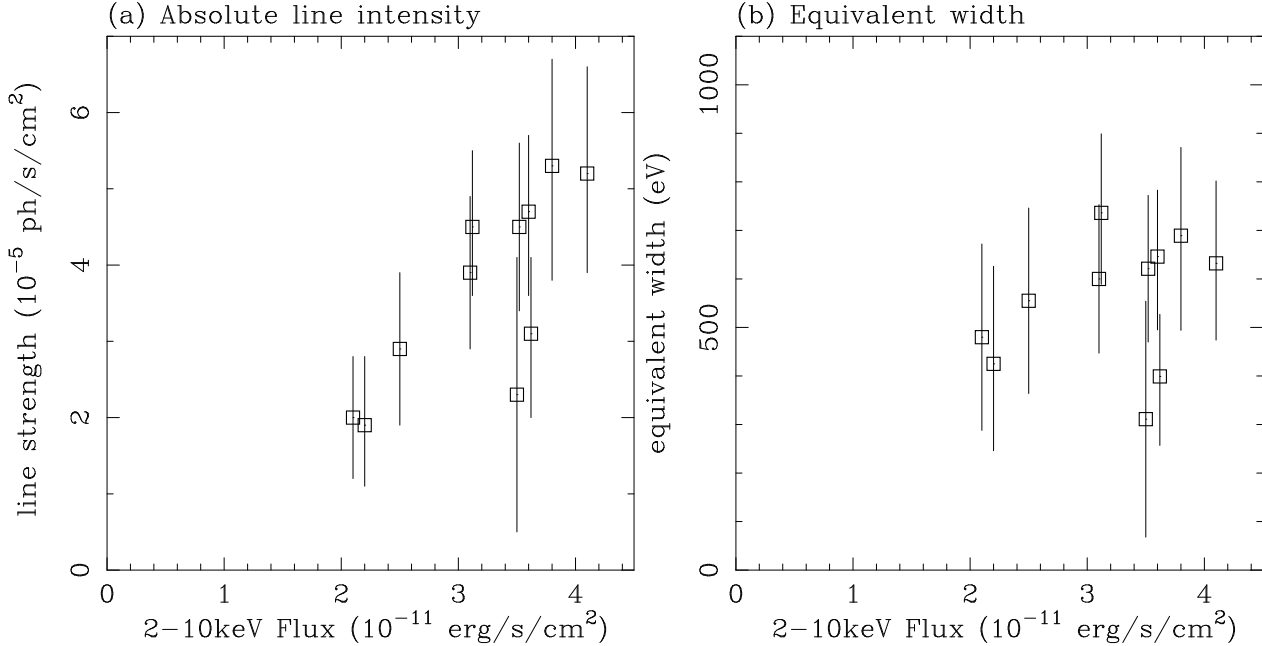


Figure 7. Result of fitting a simple absorbed power-law plus **laor** component to the 10 ksec segments of data. Panel (a) shows the absolute intensity of the **laor** component as a function of 2–10 keV flux. Note the apparent correlation of line intensity with continuum flux. Panel (b) shows the equivalent width of the **laor** component as a function of 2–10 keV flux. It can be seen that these data are consistent with a constant equivalent width. Error bars are shown at the 90% level for one significant parameter ($\Delta\chi^2 = 2.71$).

5 DISCUSSION AND CONCLUSIONS

5.1 Characteristics of the Deep Minimum and Normal states of MCG–6-30-15

The study described in Sections 3 and 4 represents the most detailed study of the Deep Minimum state of MCG–6-30-15 to date. We have come to two important conclusions.

(i) We have demonstrated the robustness of the extremely broadened disk reflection features reported in Paper I. We employ the generalized thin disk model of Agol & Krolik (2000), which includes a torque applied at the radius of marginal stability $r = r_{\text{ms}}$, and find that this inner torque is dominating the energetics of the system. In other words, the Deep Minimum disk is shining via the extraction of spin-energy from the central black hole and not through accretion.

(ii) Examination of both the difference spectra and direct spectral fits to the 10 ksec segments of data shows that the intensity of the broad disk feature is consistent with being proportional to the 2–10 keV flux. In other words, the equivalent width of the disk feature is roughly constant as the source undergoes its large amplitude variability. This is expected from the simplest X-ray reflection model.

It is important to compare and contrast these results with studies of MCG–6-30-15 in its normal state. In their paper that originally identified the Deep Minimum state, Iwasawa et al. (1996) used *ASCA* to show that the iron line profile was substantially broader in the Deep Minimum than at other times. More recently, Fabian et al. (2002; hereafter F02) examined an independent and long (350 ksec) *XMM-Newton* observation of MCG–6-30-15 which mostly caught it in its normal flux state. In agreement with the expectation from Iwasawa et al. (1996), F02 found the iron line profile

to be generally narrower than in the Deep Minimum state of Paper I, although they clearly noted an extreme red-tail extending down to ~ 3 keV. Fitting the iron line with a near-extreme Kerr black hole model ($a = 0.998$) using a broken-powerlaw emissivity profile indicated a rather flat emissivity profile ($\beta \sim 2.5$) for $r > 6r_g$, breaking to a steep profile ($\beta \sim 5$) within this radius. Thus, the principal difference in the shape of the emissivity profile between the Deep Minimum and normal states of MCG–6-30-15 appears to lie beyond some radius $r \sim 6r_g$. While it is beyond the scope of this paper to fit our physical accretion disk models to the long *XMM-Newton* data set, it is clear that a torque-dominated disk around a rapidly spinning black hole cannot reproduce the normal state emissivity profile.

There are also interesting differences in the spectral variability properties of the two states. Careful analysis of the *RXTE*-PCA data for MCG–6-30-15 during the normal state clearly showed that the iron line flux underwent significant variations but was not correlated with the continuum flux (Lee et al. 2000; Reynolds 2000; Vaughan & Edelson 2001). This was confirmed in a rather direct manner by Shih, Iwasawa & Fabian (2002) who used the 910 ksec *ASCA* observation of MCG–6-30-15 to show that neither the intensity nor profile of the iron line were functions of the continuum flux. Finally, Fabian et al. (2002) and Fabian & Vaughan (2003) examined the long (350 ksec) *XMM-Newton*/EPIC data of MCG–6-30-15 in its normal state and found that the hard-band difference spectra were all well described by power-law forms. Using this fact, these authors decompose the EPIC-pn spectrum into an almost constant reflection dominated component and variable power-law component. This is clearly different to the behaviour that we find during the Deep Minimum state.

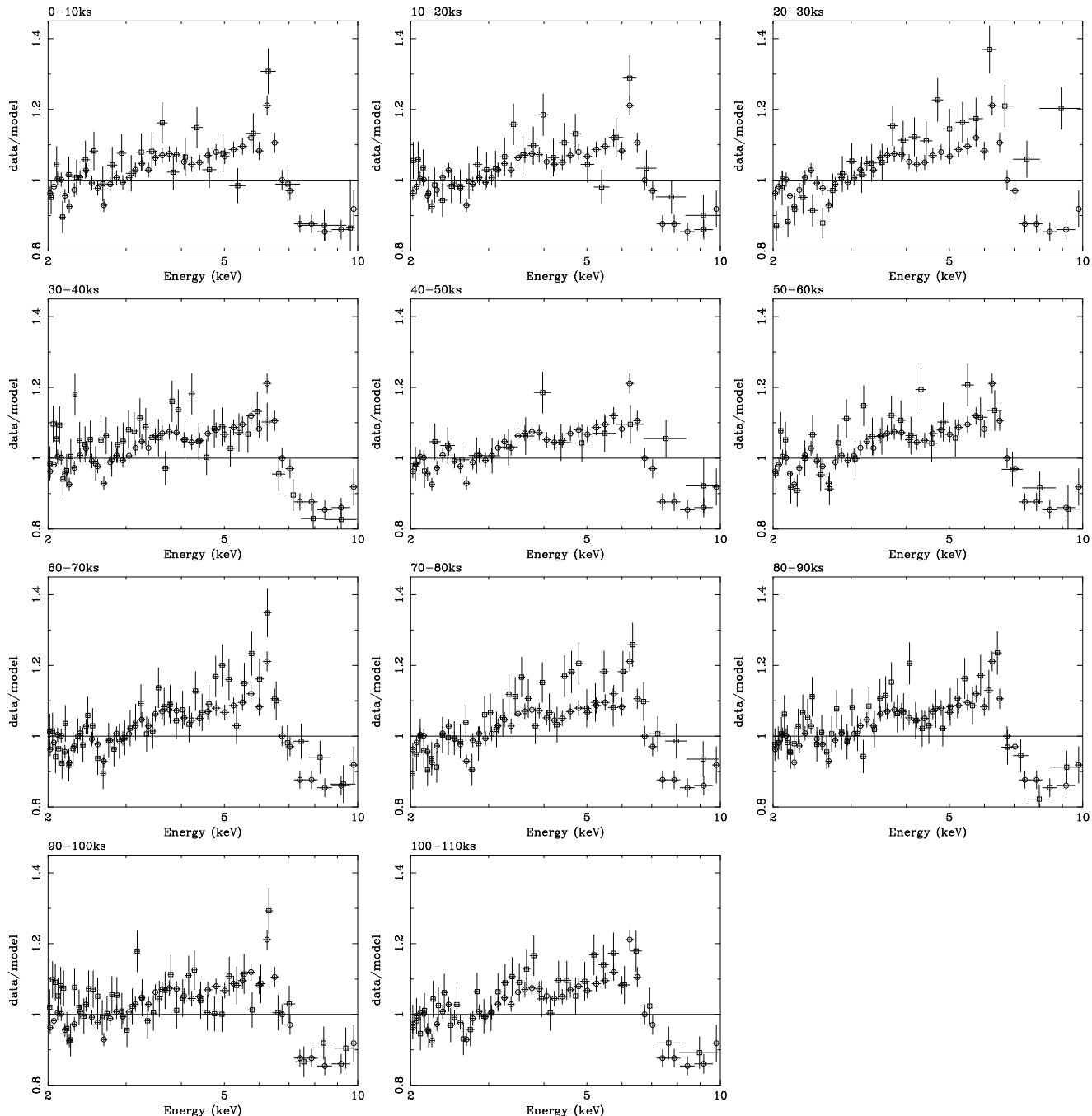


Figure 8. 2–10 keV spectra from the 10 ksec segments of data (open squares) ratioed against a simple power-law. The photon index of the power-law has been fixed to that derived from fitting to the time-averaged spectrum, $\Gamma = 1.80$. No significant changes in the profile of the disk-reflection component is found.

5.2 Implications for models of the central engine of MCG–6–30–15

5.2.1 General considerations

Finally, we discuss the implications of these results for theoretical models of the central engine. In this discussion, we shall assume that the hard-band X-ray spectral features arise from X-ray illumination of a flat accretion disk orbiting a rapidly-rotating black hole in the prograde sense in the $\theta = \pi/2$ plane. We shall also assume that the steep

emissivity profile of the inner disk is due to a violation of the standard zero-torque boundary condition at $r = r_{\text{ms}}$.

We must note that the physics of the inner disk boundary is still very uncertain and the subject of current work and debate. The motivation behind the TORQUED model of Section 3.4 was the presence of a magnetic connection between the inner disk and either the plunging region (Agol & Krolik 2000) or the rotating (stretched) event horizon itself (Li 2002). However, all aspects of this scenario have been challenged and debated. Li (2003) analyzed the structure of the magnetic field within the plunging region and argued

that the magnetic connection is too weak for the plunging region to influence the rest of the disk. However, these arguments are tempered by the fact that it seems to be rather easy to torque the disk with the plunging regions in simulated accretion disks (e.g., Hawley & Krolik 2001; Reynolds & Armitage 2002). On a different note, Merloni & Fabian (2003) have used the Merloni (2003) model for the energization of the disk corona to argue that the inner corona is strongly suppressed by disk torquing. In other words, while the dissipation profile in a torqued disk can be very centrally concentrated, it might be hard to translate this into a centrally concentrated X-ray emission pattern. Instead, they suggest that magnetic connections with the plunging region or rotating black hole energize the corona directly. A possible problem with this scenario is the requirement that the corona can transport the angular momentum released by the plunging region or black hole. Finally, Williams (2003) has challenged the notion that magnetic fields are relevant for energizing the innermost disk. She shows that Penrose scattering processes (Penrose 1969; Williams 1995) can lead to a non-magnetic spin energy extraction mechanism.

It is beyond the scope of this (observational) paper to address these physical processes in any detail. For now, we loosely refer to all of the above models and variants as “torqued disk models”, and assume that some form of interaction with the plunging region or ergosphere of the black hole is energizing the inner disk/corona and producing the steep emissivity profile seen in the observations.

5.2.2 Possible scenarios for state transitions

We can organize possible scenarios for Deep Minimum state transitions by considering the three components of the X-ray continuum that might be relevant to inner disk X-ray reflection; (1) the normal accretion-powered X-ray emission from the corona of the accretion disk, (2) the torque-powered X-ray emission from the corona of the inner accretion disk, and (3) X-ray emission from a high latitude source (maybe the base of a Blandford-Znajek powered jet) near the black hole spin-axis (we shall refer to this as the jet-component, although this emitting material may not necessarily be moving rapidly). We can then elucidate three scenarios for normal/Deep-Minimum state changes in MCG–6-30-15 by considering the dominance of these three X-ray continuum components.

(i) *Constant-torque, variable-accretion case:* Suppose that the inner disk torque is long-lived and changes in inner disk accretion rate drive the observed changes. In particular, the Deep Minimum state would correspond to a temporary but dramatic decline in the accretion rate through the inner disk. This naturally explains the drop in continuum flux during Deep Minima as well as the broadening of the disk reflection features. On the other hand, this scenario does not straightforwardly explain why the strength of the X-ray reflection features appears to saturate in the normal state (i.e. maintain a constant flux rather than equivalent width). As discussed by Reynolds (2000) and Lee et al. (2000), flux-correlated ionization changes in the disk surface might be responsible for this effect. A potentially more problematic issue for this scenario is the rate at which MCG–6-30-15 can transit into a Deep Minimum state. One

naively expects the accretion rate to change on the viscous timescale $t_{\text{visc}} = (r/h)^2 \alpha^{-1} t_{\text{dyn}}$, where r is the radius of the disk, $h \sim 0.1r$ is its thickness, t_{dyn} is the dynamical timescale and $\alpha = 0.1\alpha_{0.1}$ (with $\alpha_{0.1} \sim 0.1 - 1$) is the usual dimensionless angular momentum transport parameter of Shakura & Sunyaev (1973). If the mass of the black hole is $M = 10^6 M_6 M_\odot$ (with $M_6 \sim 1-10$; Reynolds 2000) we can deduce $t_{\text{dyn}} \sim 50 M_6$ s. Thus, we have $t_{\text{visc}} \sim 50 M_6 \alpha_{0.1}$ ksec. Although the actual time required to transit to the Deep Minimum state is poorly characterized, the *ASCA* study of Iwasawa et al. (1996) suggest that it is rather more rapid (< 5 ksec). Thus, this model has may have problems reproducing the rapid transition. More detailed modelling, which is beyond the scope of this paper, is required to assess whether changes in accretion rate can really occur on such rapid timescales.

(ii) *Sporadic-torque, constant-accretion case:* Motivated by the timescales noted above, we consider a model in which the accretion rate in the inner disk is constant, but the torque exerted on the inner boundary by the plunging region or the spinning black hole is sporadic on a short timescale. In this case, the Deep Minimum state corresponds to rather rare intervals (duty cycle of $\sim 20\%$) in which the torque is “engaged” and strongly energizing the inner disk (the fact that F02 also observe a steep emissivity profile in the very innermost disk suggests that the torque is engaged, albeit more weakly, even in the normal state). This model successfully explains the changes in the line profile and (by construction through the assumed time-dependence of the torque) the rapid transition timescale. As before, flux-correlated ionization changes would have to be invoked to explain the saturation of the reflection features seen in the normal state. However, all other things being equal, the torqued disk would be expected to be more luminous than the untorqued disk due to the work done by the torque. This is in contrast with the observed continuum drop when the source enters the Deep Minimum state. However, more theoretical work on the physics of sporadically-torqued accretion disks is required to assess the true time-dependence of the luminosity.

(iii) *Time variable height of a jet X-ray source:* As discussed by Fabian & Vaughan (2003), an interesting possibility is that a classical accretion powered disk corona is (even if it exists) unimportant for producing the X-ray reflection features. Following the work of Martocchia & Matt (1996) and Martocchia, Matt & Karas (2002), Fabian & Vaughan (2003) suggest that the X-ray source is located close to the spin-axis of the black hole and at some height from the accretion disk. If one further supposes that the long term ($f < 10^{-4}$ Hz) variability of MCG–6-30-15 is driven by changes in the height and not intrinsic luminosity of this source, general relativistic effects (predominantly gravitational lightbending) can reproduce the observed relation of continuum and X-ray reflection intensities. We can extend the Fabian & Vaughan (2003) scenario into the Deep Minimum state in two ways. Firstly, there might be a separate X-ray component due to the inner disk torque (which would be emitted in a disk corona) that is responsible for the extreme red wing seen at all times in this source. The Deep Minimum state then corresponds to times when the jet source fades to low levels. Secondly, it is possible that there is only one X-ray emitting component. In the normal state, this is the jet

component as discussed by Martocchia & Matt (1996) and Fabian & Vaughan (2003). The Deep Minimum state could correspond to times when the height of the jet component goes to zero in a continuous manner, i.e., the jet component touches-down on the disk and transits over to become a viscously mediated torque-component. This latter event might accompany a change in the structure of the black hole magnetosphere.

The key to distinguishing between these models is application of physical disk models similar to those described in this paper to all available high-quality data of MCG–6-30-15 and similar sources. This will allow us to determine observationally whether the torqued component varies dramatically when the source enters into a Deep Minimum state. We also need more realistic spectral models so that the physics of the accretion disk can be probed with confidence. Obvious improvements are to develop models in which the black hole spin is a free parameter of the fit (since we have no right to believe that all real black holes have dimensionless spin parameters of $a = 0.998$) which also take into account that the inner edge of the fluorescing part of an accretion disk is not sharp (Krolik & Hawley 2002). MHD simulations will be invaluable for guiding development of such models.

It might be difficult to disentangle the possible role of an on-axis jet using current data alone. Observationally decomposing the X-ray continuum into its coronal and jet components may have to await the next generation of large-area observatories (principally Constellation-X and XEUS) which will allow one to assess the time delay between rapid X-ray variability and responses in the X-ray reflection spectrum. A measurement of this reverberation timescale would place strong constraints on the location of the X-ray source. We note that an X-ray source close to the spin axis of the black hole is the most favourable geometry for probing very strong relativistic effects (including a robust measure of the black hole's spin parameter) through X-ray iron line reverberation (Stella 1990; Matt & Perola 1992; Campana & Stella 1993, 1995; Reynolds et al. 1999; Young & Reynolds 2000).

ACKNOWLEDGMENTS

We thank Andy Fabian, David Garofalo, Julian Krolik, Cole Miller, and Andy Young for insightful and stimulating discussions throughout the course of this work. We also thank the anonymous referee for their thoughtful comments which lead to a dramatic improvement in the presentation of Section 3.4. We gratefully acknowledge support from the National Science Foundation under grant AST0205990 (CSR), AST9876887 (MCB) and AST0307502 (MCB).

REFERENCES

- Agol, E., & Krolik, J. H., 2000, *ApJ*, 528, 161
 Arnaud, K.A., in: *Astronomical Data Analysis Software and Systems V* (eds. J.H. Jacoby and J. Barnes), ASP Conf. Ser. 101, San Francisco: Astron. Soc. Pacific, p. 17
 Ballantyne D.R., Ross R.R., Fabian A.C., 2001, *MNRAS*, 327, 10
 Blandford, R. D., & Znajek, R. L., 1977, *MNRAS*, 179, 433
 Branduardi-Raymont, G., Sako, M., Kahn, S. M., Brinkman, A. C., Kaastra, J. S., & Page, M. J., 2001, *A&A*, 365, L140
 Campana S., Stella L., 1993, *MNRAS*, 264, 395
 Campana S., Stella L., 1995, *MNRAS*, 272, 585
 Cunningham C.T., 1975, *ApJ*, 202, 788
 Dabrowski, Y., Fabian, A. C., Iwasawa, K., Lasenby, A. N., & Reynolds, C. S., 1997, *MNRAS*, 288, L11
 Eckart A., Genzel R., 1997, *MNRAS*, 284, 576
 Eckart A., Genzel R., Ott T., Schödel R., 2002, *MNRAS*, 331, 917
 Elvis M., Wilkes B.J., Lockman F.J., 1989, *AJ*, 97, 777
 Fabian A.C., Vaughan S., 2003, *MNRAS*, in press (*astro-ph/0301588*)
 Fabian, A. C., Iwasawa, K., Reynolds, C. S., & Young, A. J., 2000, *PASP*, 112, 1145
 Fabian A.C. et al., 1995, *MNRAS*, 277, L11
 Fabian A.C. et al., 2002, *MNRAS*, 331, L35 (F02)
 Ferrarese L., Merritt D., 2000, *ApJL*, 539, L9
 Ford H.C. et al., 1994, *ApJL*, 435, L27
 Gammie C.F., 1999, *ApJ*, 522, L57
 Gebhardt K., et al., 2000, *ApJL*, 539, L13
 George I.M., Turner T.J., Netzer H., Nandra K., Mushotzky R.F., Yaqoob T., 1998, *ApJ*, 493, 91.
 Ghez A., Klein B.L., Morris M., Becklin E.E., 1998, *ApJ*, 509, 687
 Ghez A., Morris M., Becklin E.E., Tanner A., Kremenek T., 2000, *Nature*, 407, 349
 Ghez A. et al., 2003, *ApJ*, 586, L127
 Greenhill L., Henkel C., Becker R., Wilson T.L., Wouterloot J.G.A., 1995, *A&A*, 304, 21
 Harms R.J. et al., 1994, *ApJL*, 435, L35
 Hawley J.F., Krolik J.H., 2001, *ApJ*, 548, 348
 Iwasawa, K., et al., 1996, *MNRAS*, 282, 1038
 Krolik, J. H., 1999, *ApJ*, 515, L73
 Krolik J.H., Hawley J.F., 2002, *ApJ*, 573, 754
 Laor, A., 1991, *ApJ*, 376, 90
 Lee J.C., Fabian A.C., Reynolds C.S., Brandt W.N., Iwasawa K., 2000, *MNRAS*, 318, 857
 Lee, J. C., Ogle, P. M., Canizares, C. R., Marshall, H. L., Schulz, N. S., Morales, R., Fabian, A. C., & Iwasawa, K., 2001, *ApJ*, 554, L13
 Li L.X., 2002, *ApJ*, 567, 463
 Li L.X., 2003, *Phys. Rev. D*, 67, 4007
 Lynden-Bell D., 1969, *Nature*, 223, 690
 Magdziarz P., Zdziarski A.A., 1995, *MNRAS*, 273, 837
 Martocchia A., Matt G., 1996, *MNRAS*, 282, L53
 Martocchia A., Matt G., Karas V., 2002, *A&A*, 383, L23
 Mason K.O. et al., *ApJ*, 582, 95
 Matt G., Perola G. C., 1992, *MNRAS*, 259, 433
 Merloni A., 2003, *MNRAS*, 341, 1051
 Merloni A., Fabian A.C., 2003, *MNRAS*, in press (*astro-ph/0303143*)
 Myoshi M., Moran J., Herrnstein J., Greenhill L., Nakai N., Diamond P., Inoue M., 1995, *Nature*, 373, 127
 Nandra K., Pounds K.A., 1992, *Nat*, 359, 215
 Novikov I.D., Thorne K.S., in *Black Holes*, eds. C.DeWitt & D.DeWitt, 1974, pp.343.
 Page D.N., Thorne K.S., 1974, *ApJ*, 191, 499
 Penrose R., 1969, *Rivista Del Nuovo Cimento: Numero Speciale*, 1 252
 Protassov R., van Dyk D.A., Connors A., Kashyap V.L., Siemiginowska A., 2002, *ApJ*, 571, 545
 Reynolds C.S., 1997, *MNRAS*, 286, 513
 Reynolds C.S., 2000, *ApJ*, 533, 811
 Reynolds, C. S., & Begelman, M. C., 1997, *ApJ*, 487, 109
 Reynolds C.S., Armitage P.J., 2002, *ApJ*, 561, L81
 Reynolds C.S., Nowak M.A., 2003, *Physics Reports*, 377, 389
 Reynolds C.S., Ward M.J., Fabian A.C., Celotti A., 1997, *MNRAS*, 291, 403
 Reynolds C.S., Young A.J., Begelman M.C., Fabian A.C., 1999, *ApJ*, 514, 164

- Salpeter E.E., 1964, *ApJ*, 140, 796
Sako M. et al., 2003, *ApJ*, submitted
Schödel R. et al., 2002, *Nature*, 2002, 419, 694
Shakura N.I., Sunyaev R., 1973, *A&A*, 24, 337
Shih D.C., Iwasawa K., Fabian A.C., 2002, *MNRAS*, 333, 687
Spergel D.N. et al., 2003, *ApJ*, in press (astro-ph/0302209)
Stella L., 1990, *Nat*, 344, 747
Tanaka, Y., et al., 1995, *Nature*, 375, 659
Titarchuk L., 1994, *ApJ*, 434, 313
Vaughan S., Edelson R., 2001, *ApJ*, 548, 694
Williams R.K., 1995, *Phys. Rev. D*, 51, 5387
Williams R.K., 2003, *ApJ*, in press (astro-ph/0210139)
Wilms, J., Allen, A., & McCray, R., 2000, *ApJ*, 542, 914
Wilms J., Reynolds C.S., Begelman M.C., Reeves J., Molendi S.,
Staubert R., Kendziorra E., 2001, *MNRAS*, 328, L27 (Paper
I)
Young A.J., Reynolds C.S., 2000, *ApJ*, 529, 101
Zeldovich Y.B., 1964, *Sov. Phys.-Dokl.*, 1548, 811